doi:10.1006/jmbi.2000.3883 available online at http://www.idealibrary.com on IDEAL® J. Mol. Biol. (2000) 300, 619–632

JMB

Binding of Retinol Induces Changes in Rat Cellular Retinol-binding Protein II Conformation and Backbone Dynamics

Jianyun Lu[1], Chan-Lan Lin[1], Changguo Tang[2], Jay W. Ponder[2] Jeff L. F. Kao[3], David P. Cistola[2] and Ellen Li[1,2]*

[1]*Departments of Internal Medicine, and*

[2]*Biochemistry & Molecular Biophysics and*

[3]*Chemistry, Washington University School of Medicine St. Louis, MO 63110, USA*

**Corresponding author*

The structure and backbone dynamics of rat holo cellular retinol-binding protein II (holo-CRBP II) in solution has been determined by multidimensional NMR. The final structure ensemble was based on 3980 distance and 30 dihedral angle restraints, and was calculated using metric matrix distance geometry with pairwise Gaussian metrization followed by simulated annealing. The average RMS deviation of the backbone atoms for the final 25 structures relative to their mean coordinates is 0.85(±0.09) Å. Comparison of the solution structure of holo-CRBP II with apo-CRBP II indicates that the protein undergoes conformational changes not previously observed in crystalline CRBP II, affecting residues 28-35 of the helix-turn-helix, residues 37-38 of the subsequent linker, as well as the β-hairpin C-D, E-F and G-H loops. The bound retinol is completely buried inside the binding cavity and oriented as in the crystal structure. The order parameters derived from the ^{15}N T_1, T_2 and steady-state NOE parameters show that the backbone dynamics of holo-CRBP II is restricted throughout the polypeptide. The T_2 derived apparent backbone exchange rate and amide ^1H exchange rate both indicate that the microsecond to second timescale conformational exchange occurring in the portal region of the apo form has been suppressed in the holo form.

Keywords: cellular retinol-binding protein; lipid-binding protein; NMR; structure; lipid transport

Introduction

Cellular retinol-binding protein II (CRBP II) is a 15 kDa cytosolic protein that binds all-*trans*-retinol, and all-*trans*-retinaldehyde but not retinoic acid (Li & Norris, 1996). It is a member of a large family of intracellular lipid-binding proteins that bind fatty acids, retinoids and bile acids. Expression of CRBP II is restricted to the small intestinal villus cells and to the neonatal hepatocyte, whereas its close homologue, cellular retinol-binding protein (CRBP), is distributed widely throughout the body. CRBP has recently been shown to be essential for storage of vitamin A in the liver (Ghyselinck *et al*., 1999). Studies of null mutant CRBP II mice are currently underway (E *et al*., 1999). In addition to the distinct patterns of gene expression, there are differences in how CRBP and CRBP II interact with ligands and with retinoid metabolizing enzymes such as lecithin:retinol acyl transferase, which suggest that the physiological role of CRBP II is distinct from that of CRBP.

Retinol dissociates from CRBP II far more readily than it does from CRBP (Li *et al*., 1991). Transfer of retinol from CRBP II to lipid membranes appears to occur by a diffusional mechanism, whereby retinol spontaneously dissociates from the binding pocket, and diffuses through the aqueous medium prior to reaching the acceptor

Abbreviations used: COSY, correlation spectroscopy; CRABP, cellular retinoic acid-binding protein; CRBP, cellular retinol-binding protein; CSI, chemical shift index; DQF, double quantum filtered; HMQC, heteronuclear multiple-quantum correlation; HSQC, heteronuclear single-quantum correlation; IFABP, intestinal fatty acid-binding protein; LRAT, lecithin-retinol acyltransferase; NOE, nuclear Overhauser effect; NOESY, nuclear Overhauser and exchange spectroscopy; RMSD, root-mean-square deviation; TOCSY, total correlation spectroscopy.

E-mail address of the corresponding author: eli@imgate.wustl.edu

0022-2836/00/030619–14 $35.00/0

lipid vesicle. In contrast, transfer of retinol from CRBP appears to occur by a collisonal mechanism, whereby transfer takes place only after direct contact between CRBP and the acceptor vesicle (Herr *et al*., 1999). How retinol can enter and leave CRBP II is not apparent from the apo and holo crystal structures of this protein (Winter *et al*., 1993). CRBP II binds all-*trans*-retinol with high affinity within a large cavity formed by a ten-stranded antiparallel β-sheet (A-J) and capped on one side by two α-helices. The crystal structures of apo and holo-CRBP II are virtually identical and their binding cavities are both virtually solvent-inaccessible. Increase in size-exclusion retention time (Herr & Ong *et al*., 1992) and reduced sensitivity to limited proteolysis (Jamison *et al*., 1994) on binding all-*trans*-retinol, indicate that CRBP II conformation is altered by ligand binding. These differences in conformation may not be sampled adequately in the crystalline form. To study the solution conformation and backbone dynamics of CRBP II, we have performed a series of multidimensional, high-resolution NMR experiments on uniformly ^{13}C and ^{15}N-enriched *Escherichia coli*-derived rat CRBP II. We have recently reported the solution structure and backbone dynamics of apo-CRBP II, which revealed an increased accessibility to the binding pocket compared to that previously observed in the crystal structure (Lu *et al*., 1999). We now report the solution structure and backbone dynamics of CRBP II complexed with all-*trans*-retinol. The results indicate that binding of all-*trans*-retinol induces significant changes in protein conformation and backbone dynamics.

Results and Discussion

Protein resonance assignments

In contrast to the apoprotein, in which a number of backbone ^{1}HN resonances were missing due to fast solvent exchange, the backbone ^{1}HN resonances of all but the first two residues were observed in the HNCO and CBCA(CO)NNH spectra of ^{13}C, ^{15}N-enriched holo-CRBP II complexed with natural abundance all-*trans*-retinol collected at pH 7.4. Consequently, a complete sequence-specific backbone resonance assignment was accomplished using six scalar coupling-based experiments (detailed in Materials and Methods) at pH 7.4. All aliphatic side-chain ^{1}H and ^{13}C chemical shifts were assigned except for those of M1, H^{ε} and C^{ε} of K53, and H^{γ} and C^{γ} of R83. Most of the aromatic protons and side-chain amide protons were assigned using intra-residue NOE connectivity. Since the resonance assignments for the apoprotein were made at pH 6.5, the backbone and aliphatic side-chain ^{1}H and ^{15}N chemical shifts of holo-CRBP II complexed with all-*trans*-retinol were also measured at pH 6.5. The chemical shifts measured at both pH values differ by less than 0.1 ppm in the ^{1}H and by less than 0.8 ppm in the ^{15}N dimension.

Like apo-CRBP II, multiple backbone amide ^{1}H, ^{15}N resonances were observed for a number of residues at both pH 7.4 and 6.5, such as residues 3-5, 19, 23, 27, 75, 80, 90, 106, 109 and 121. The chemical shift difference was small in all cases, suggesting that the corresponding conformational change might be subtle. No exchange cross-peak was observed for these residues, indicating that the exchange was slow under the experimental conditions. This is different from the observation for apo-CRBP II, in which exchange cross-peaks were observed for a number of residues (Lu *et al*., 1999).

Ligand resonance assignments

A ^{1}H-^{13}C HMQC spectrum collected on CRBP II-bound (1,4,5,8,9,16,17,18,19-^{13}C) all-*trans*-retinol aided in the assignment of ligand protons and their attached ^{13}C resonances (see Figure 1). The olefinic region of this spectrum (see Figure 1(a)) shows a single resonance corresponding to CH(8). The methyl resonances CH_3(16,17), CH_3(18) and CH_3(19) were assigned on the basis of comparisons with the aliphatic region of the HMQC spectra of CRABP I and CRABP II-bound (1,4,5,8,9,16,17,18,19-^{13}C) all-*trans*-retinoic acid (Norris *et al*., 1995) and with previously published chemical shift data (Liu & Asato, 1984). A single methylene resonance corresponding to CH_2(4) was observed in the aliphatic region of the HMQC spectrum (see Figure 1(b)).

In order to assign the remainder of the CRBP II-bound retinol proton resonances, ^{13}C-filtered DQF-COSY, TOCSY and NOESY spectra were collected on a sample of natural abundance all-*trans*-retinol bound to ^{13}C, ^{15}N-enriched CRBP II at pH 7.4 (see Figure 1(c) and (d)). Intense NOEs were observed between CH(7) and CH_3(19), CH(11) and CH_3(19), and between CH(11) and CH_3(20). NOEs were detected between CH(8) and CH(10), CH(10) and CH(12), and between CH(12) and CH(14). These data are consistent with an 8-s *trans*, 10-s *trans* and 12-s *trans* conformation of the polyene chain for CRBP II-bound retinol. Intense NOE cross-peaks between CH(8)-CH_3(16,17) and between CH(7)-CH_3(18) were observed, however no cross-peak between CH(8)-CH_3(18) and CH(7)-CH_3(16,17) was detected. This pattern is more consistent with a 6-s-*trans* conformation and distinctly different from those of intramolecular NOESY peaks observed for CRABP I and CRABP II-bound retinoic acid (Norris *et al*., 1995).

Secondary structure derived from the chemical shift and NOE

The consensus chemical shift index of holo-CRBP II complexed with all-*trans*-retinol was calculated as described by Wishart & Sykes (1994). The results are consistent with a secondary structure

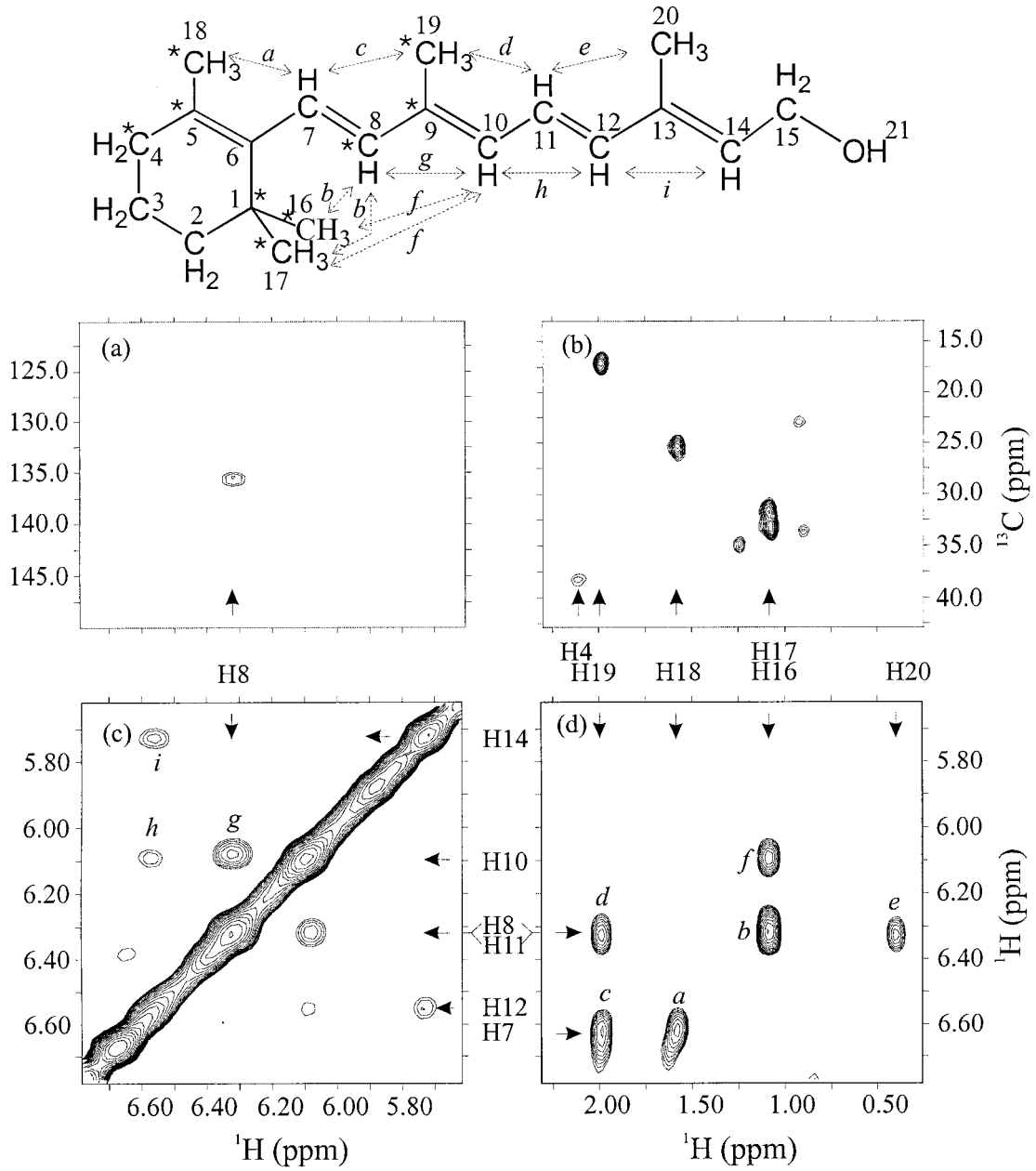

Figure 1. (a) The olefinic region and (b) the aliphatic region of the HMQC spectrum recorded on a sample of natural abundance CRBP II complexed with ligand **2** at 25 °C and pH 7.4. The three unsigned small peaks to the left and right of H17/H16 in panel (b) are likely the protein signals. (c) The respective olefinic proton region and (d) the aromatic-to-aliphatic proton region of the ^{13}C,^{15}N double-half-filtered NOE spectrum recorded on a sample of uniformly ^{13}C,^{15}N-enriched CRBP II complexed with natural abundance all-*trans*-retinol. The structure of all-*trans*-retinol is depicted at the top, the positions of ^{13}C enrichment in ligand **2** are indicated with an asterisk (*), and the observed inter-proton NOEs are indicated with broken lines and arrows.

containing two short α-helices and ten β-strands. In contrast, the consensus shift indices of apo-CRBP II are consistent with only a single α-helix. The NOE analysis was carried out to determine secondary structure and confirms the secondary structure derived by the chemical shift index method. The β-strands A to D form one part of the antiparallel β-sheet, and the β-strands E to J form the other part. Intrahelical NOE contacts were observed in two regions encompassing residues 18-23 and 28-35.

Chemical shift map

The root-mean-square (RMS) weighted difference of the amide proton and nitrogen chemical shifts of CRBP II upon binding of all-*trans*-retinol at pH 6.5 and at pH 7.4 are plotted by residue in

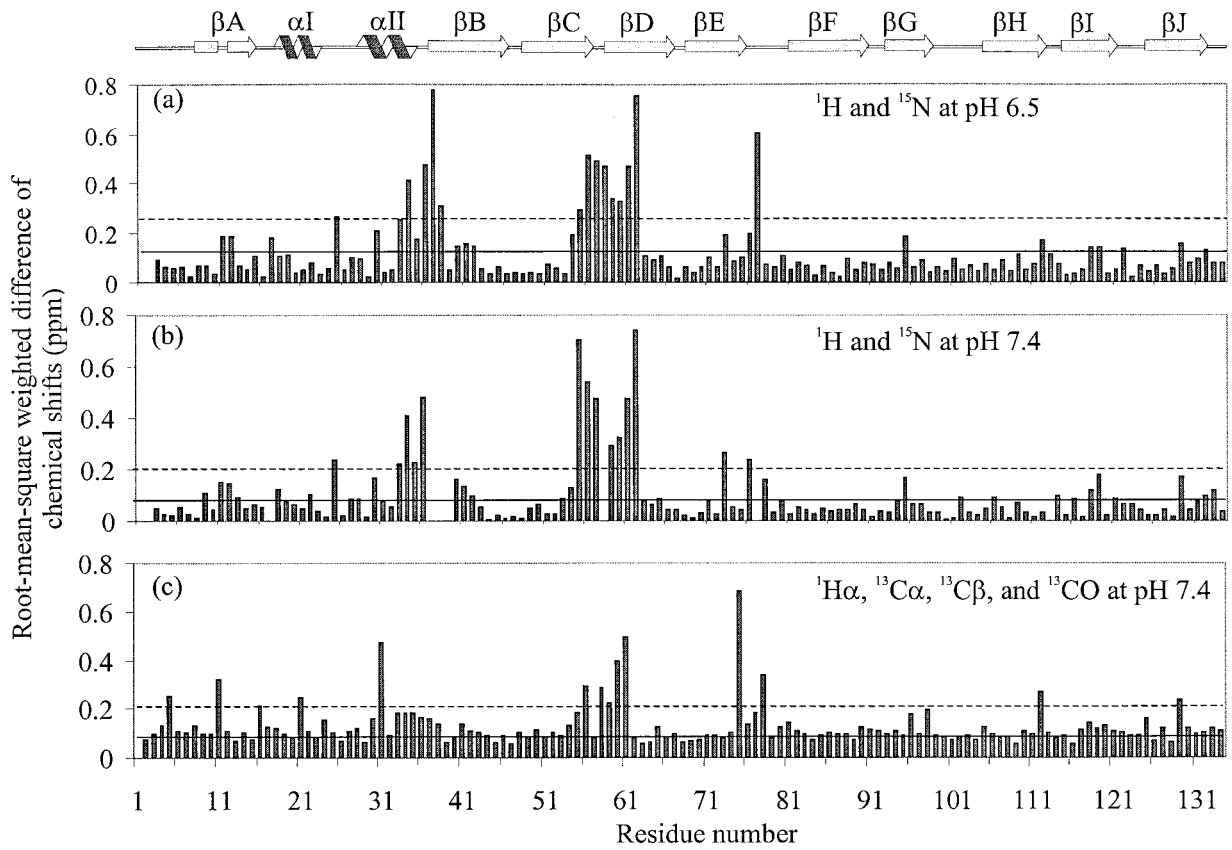

Figure 2. Root-mean-square weighted difference of backbone ^{1}HN and ^{15}N chemical shifts between holo and apo-CRBP II at (a) pH 6.5 and (b) pH 7.4, i.e. $RMSD = \sqrt{(((\delta HN^{apo} - \delta HN^{holo})^2 + ((\delta N^{apo} - \delta N^{holo})/5)^2)/2)}$, where $\delta HN^{apo/holo}$ and $\delta HN^{apo/holo}$ are the HN and N chemical shifts of apo and holo-CRBP II. (c) RMS weighted difference of $^{1}H^{\alpha}$, $^{13}C^{\alpha}$, $^{13}C^{\beta}$ and ^{13}CO chemical shift between holo and apo-CRBP II at pH 7.4, i.e. $RMSD = \sqrt{(((\delta H\alpha^{apo} - \delta H\alpha^{holo})^2 + ((\delta C\alpha^{apo} - \delta C\alpha^{holo})/5)^2 + ((\delta C\beta^{apo} - \delta C\beta^{holo})/5)^2 + ((\delta CO^{apo} - \delta CO^{holo})/5)^2)/4)}$. The continuous and broken lines are the mean and one standard deviation limit, respectively. Note that the average absolute differences of ^{1}H, ^{13}C and ^{15}N chemical shifts are 0.09, 0.53 and 0.79 ppm, respectively, at pH 7.4. In order to permit an approximately even contribution of the ^{1}H and ^{13}C or ^{15}N chemical shift differences to the RMS difference, a scaling factor of 5 used in the literature (Pellecchia *et al.*, 1999) has been adopted here to scale down the ^{13}C and ^{15}N chemical shift differences.

Figure 2(a) and (b), respectively. The perturbations are non-uniform along the length of the protein. The largest changes are observed in residues 34 and 36-38 at the end of the second helix and the beginning of the β-strand B, residues 56-62 in the β-hairpin C-D loop and residue 77 in the β-hairpin E-F loop. A complete comparison could not be made at pH 7.4, since a number of resonances were missing from the spectrum of apo-CRBP II due to fast exchange with solvent. However, there is little perturbation of the chemical shifts corresponding to residues within the β-barrel, including Gln109, whose side-chain amide group forms a hydrogen bond with the hydroxyl group of the retinol in the crystal structure. Instead, the chemical shift perturbations map to regions of the protein that correspond to the putative portal region of the protein, framed by α-helix II, the βC-βD turn and the βE-βF turn. A similar pattern was observed for the chemical shift perturbations in other main-chain and β-carbon atoms (see Figure 2(c)). Proximity to the polyene chain could potentially account for some of the chemical shift changes observed in the βC-βD turn. However, large chemical shift perturbations are observed in residues (36-38 and 75) that are not predicted to be in close proximity to the bound ligand in the crystal structure. These changes are more likely due to conformational changes occurring upon ligand binding in this region of the protein.

NMR structure of holo-CRBP II: comparison with the X-ray structure of holo-CRBP II

The structure calculations of holo-CRBP-II were carried out using TINKER, a software package for molecular mechanics and dynamics. The protocol was the same as that used for apo-CRBP-II (Lu *et al.*, 1999) and for the holo and apo intestinal fatty acid-binding protein (Hodsdon *et al.*, 1996;

Hodsdon & Cistola, 1997a). The protocol employs metric matrix distance geometry with pairwise Gaussian metrization followed by simulated annealing. The unique distance geometry algorithm implemented in TINKER overcomes the sampling and scaling problems of earlier distance geometry methods and is computationally more efficient. Currently, many NMR structures are calculated using robust torsion-space molecular dynamics algorithms as implemented in DYANA (Güntert *et al*., 1997) and XPLOR/CNS (Stein *et al*., 1997.). However, the distance geometry method used in TINKER has a distinct advantage for the calculation of molecular complexes. The ligand and protein atoms are embedded simultaneously, determining the global structure of the ligand-protein complex that is subsequently refined by simulated annealing. By contrast, torsion space methods calculate the protein structure without the ligand atoms present. After the protein structure is determined, the ligand must be introduced by a separate docking procedure, leading to the possibility of sampling or convergence problems in both stages of the procedure.

The final 25 NMR structures of holo-CRBP II were calculated from 3980 unique distance restraints, averaging 29.7 distance restraints per residue, after exclusion of the N-terminal residue M1. A stereodiagram of the final 25 NMR structures superimposed on the X-ray structure of holo-CRBP II is shown in Figure 3(a), and a ribbon diagram of the mean coordinates of the NMR structure ensemble is shown in Figure 3(b). The restraint and structure statistics of the NMR ensemble are listed in Table 1. The overall RMS deviation of the 25 structures from the mean structure is 0.85(±0.09) Å for the main-chain heavy atoms and 1.50(±0.12) Å for the side-chain atoms.

The NMR structure of holo-CRBP II complexed with all-*trans*-retinol is similar to the X-ray structure (see Figure 3). Based on an optimal superposition using the entire protein sequence, the regions that are displaced by more than one standard deviation from the mean (see Figure 4(a)) are at the N terminus, the C terminus and at the β-hairpin loops, which have fewer distance restraints. The α-helix II in the solution structure is displaced relative to the crystal structure by more than one standard deviation. This is largely due to H^{α}-H^{α} NOE and other H^{α} to side-chain proton NOEs between F17 and A35, which reduced the F17H^{α}-A35H^{α} distance from 5.7-6.3 Å in the crystal structure to 4.3-5.0 Å in the NMR ensemble.

The bound retinol resides in the binding cavity located in the upper half of the protein core, as shown in Figure 3(a) and (b). The polar hydroxyl group penetrates deep into the protein core, and the β-ionone ring is proximal to the helix-turn-helix motif. Ligand-protein NOEs were observed between retinol and residues Y20, M21, L24, I26, T30, A34, L37, Q39, K41, T54, F58, R59, N60, Y61, L63, G78, W107, Q109, L118, L120 and F131 (see Figure 5). All of these residues, except for F131, contain protons that are predicted to be within 5 Å of ligand protons in the crystal structure of holo-CRBP II. No NOE was detected for residues F17, I43 or T52, which were predicted to be within 4-5 Å of the ligand. This may be because the predicted distances between ligand and protein protons are at the limit for detection, or because of side-chain motional averaging. The overall shape of the binding cavity and the orientation of the bound retinol are very similar in the NMR and X-ray structures.

The conformation of the bound retinol was determined based on a total of 98 ligand-protein restraints, and on torsion angle constraints generated by inspection of the intra-ligand NOE pat-

Table 1. NMR structure determination statistics

A. *Restraint statistics*[a]	
Distance restraints	
Total	3980 (29.7[b] restraints/residue)
Intra-protein	
Intraresidue	850
Sequential (i, $i-1$)	965
Medium range ($\mid i-j \mid \leqslant 4$)	562
Long range ($\mid i-j \mid > 4$)	1476
Intra-ligand	28
Ligand-protein	99
Dihedral angle restraints	
Φ	13
Ψ	13
Ligand (6-s, 8-s, 10-s, 12-s)	4
Intra-protein distance restraint violations	
Upper bounds	
Largest violation (Å)	0.03
No. of violations (%)	2 of 96,325[c] (0.002)
Lower bounds	
Largest violation (Å)	−0.15
No. of violations (%)	33 of 96,325[c] (0.034)
B. *Structure statistics*	
Ramachandran plot statistics[d]	Ensemble averages
Residues in allowed regions (%)	118 (97.8)
Most favored regions	65 (54.1)
Additionally allowed regions (%)	47 (38.5)
Generously allowed regions (%)	6 (5.2)
Residues in disallowed regions (%)	3 (2.2)[e]
RMS deviations from ideal covalent geometry[f]	
Bond lengths (Å)	0.022 ± 0.007
Bond angles (°)	1.8 ± 0.3
C. *Overall RMS deviations from the mean structure* (Å)[d]	
Main-chain heavy atoms	0.85 ± 0.09
Side-chain heavy atoms	1.50 ± 0.12

[a] Analyzed using AQUA v.3.0 (Laskowski *et al*., 1996).
[b] The N-terminal residue M1 is excluded.
[c] The product of the number of restraints and the number of structures (25) in the ensemble.
[d] Analyzed using PROCHECK-NMR v.3.5 (Laskowski *et al*., 1996).
[e] The residues whose Φ and Ψ angles are in the disallowed region in three or more of the 25 structures are 3, 17, 27, 57, 70, 101, 111 and 133, and in less than three structures are 2, 4, 16, 39, 48, 81-82, 92, 102-104, 114-115, 124 and 126.
[f] Analyzed using PROCHECK v.3.5 (Laskowski *et al*., 1993).

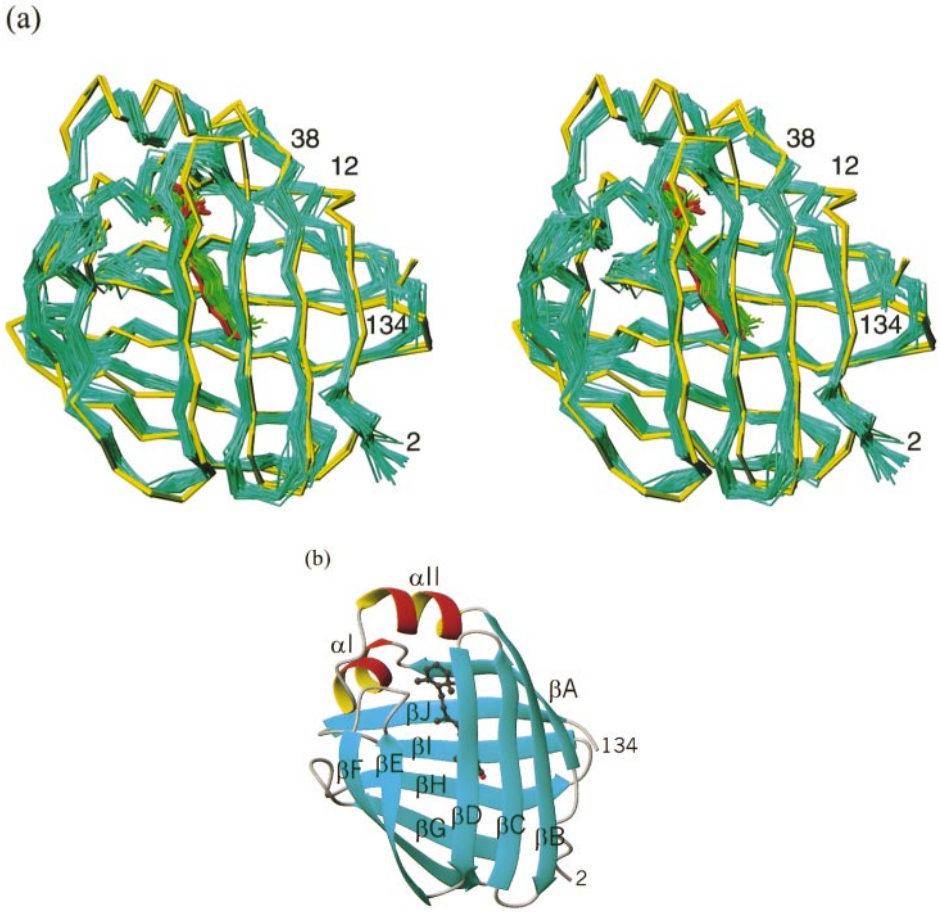

Figure 3. (a) A stereodiagram of the final 25 NMR structures of holo-CRBP II in C^{α} trace (in cyan) that are superimposed on the four molecules of the X-ray structure of holo-CRBP II (in yellow). The bound retinol is highlighted in green and red in the NMR and X-ray structures, respectively. (b) A ribbon diagram of the mean NMR structure of CRBP II-retinol (ball/stick model) complex. These molecular images and the subsequent ones were generated using MOLMOL v.2.6 (Koradi *et al.*, 1996).

tern. The RMSD of the heavy atoms of bound retinol is 0.8 Å. The polyene chain assumes an all-*trans* planar conformation. The torsion angle between the β-ionone ring and the polyene chain is in the s-*trans* conformation (−119.90(±0.04)°). The torsion angle restraints made in this structure calculation were set on the basis of the intense NOEs detected between CH(7) and CH_3(18), and between CH(8) and CH_3(16,17), and the absence of NOEs detected between CH(7) and CH_3(16,17) or CH(8) and CH_3(18). This pattern of NOEs is distinct from the pattern observed previously for CRABP II-bound retinoic acid, which was calculated to assume a skewed 6-s-*cis* conformation (−60°, Norris *et al.*, 1995). The dependence of relative NOESY cross-peak volumes on the 6-s torsion angle has been previously calculated as described by Norris *et al.* (1995). These calculations indicate that the cross-peak volumes for CH(7)-CH_3(16) and CH(8)-CH_3(18) rise rapidly when the 6-s torsion angle deviates from 180° by more than 60°. Of note, the 6-s-torsional angle for the four CRBP II molecules in crystalline holo-CRBP II were −84°, −122°, −128° and −150° (Winter *et al.*, 1993).

Two energy minima are predicted for the 6-s torsion angle between the β-ionone ring and the polyene chain. One is a broad minimum centered around a skewed s-*cis* conformation, and the second is a relatively sharp energy minimum around an s-*trans* conformation. At these orientations, there are minimal steric interactions between the CH(7) and CH(8) vinyl protons and the ring methyl protons, CH_3(16), CH_3(17) and CH_3(18). The 6-s-*trans*-conformation is predicted to be slightly less energetically favorable than the 6-s-*cis* conformation for the free ligand (Honig *et al.*, 1971). The difference in energy between these two states is small. Both conformations have been observed for retinoids in solution (Honig *et al.*, 1971) and retinoids complexed with specific binding proteins (Harbison *et al.*, 1985; Li & Norris, 1996).

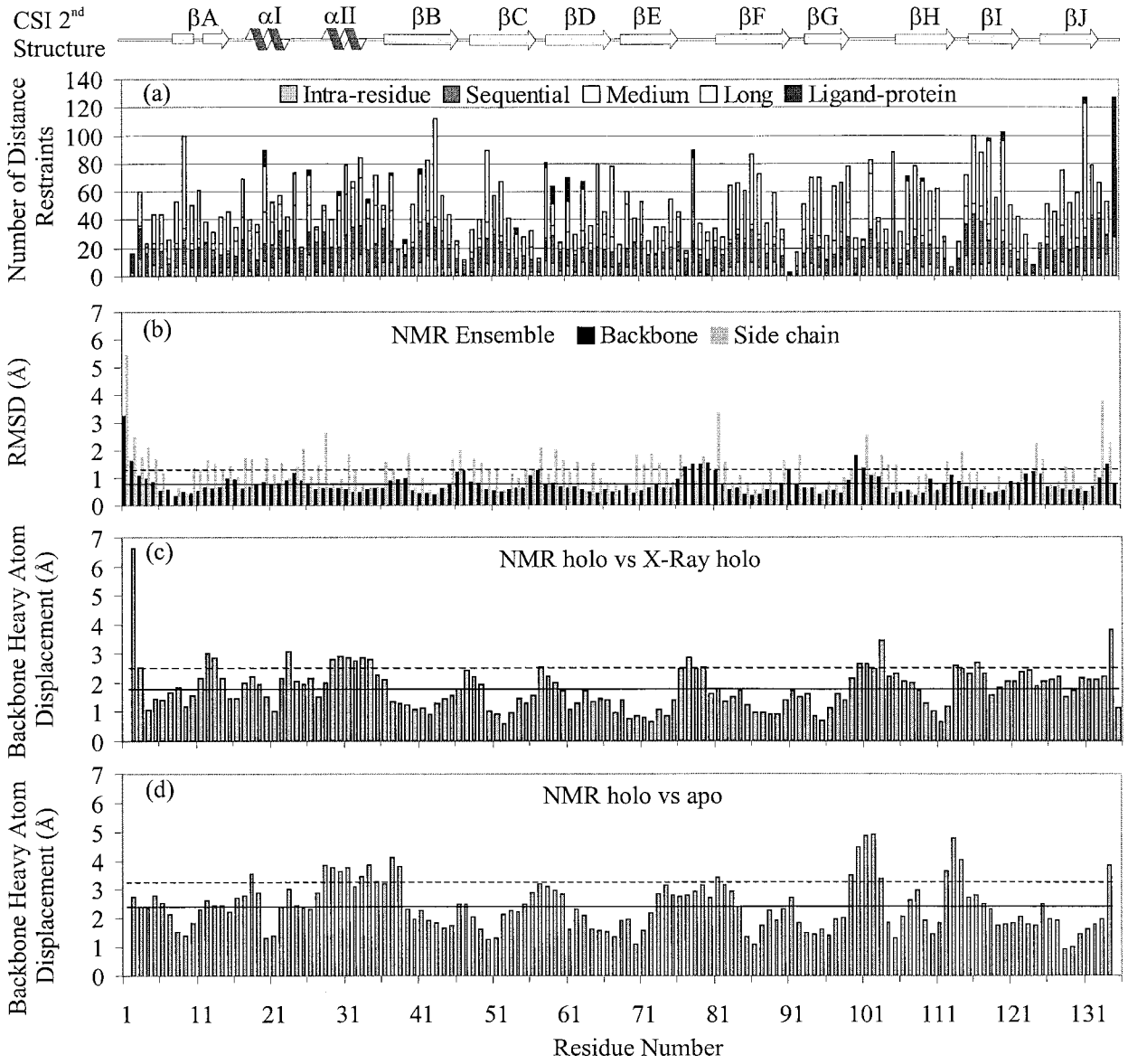

Figure 4. (a) Distribution of the distance restraints for the final 25 NMR structures. The CSI-derived secondary structure is placed on the top of the chart. (b) RMS deviations of the backbone and side-chain heavy-atom coordinates of the 25 structures to their mean coordinates (calculated with Procheck-NMR). The N terminus M1 is excluded. (c) Pairwise average backbone heavy-atom displacements of the final 25 solution structures from the crystal structures (calculated with MOLMOL v.2.6). The N terminus M1 was not visible in the crystal structure and is not included in the comparison. (d) Pairwise average backbone heavy-atom displacements of the final 25 solution structures from the solution structures of apo-CRBP II. The continuous and broken lines in (b)-(d) are the mean and one standard deviation limit, respectively.

Comparison of the NMR structure of holo-CRBP II with the NMR structure of apo-CRBP II

The structure of holo-CRBP II with an average RMSD of 0.85 Å is better defined than the apo form, which had an average RMSD of 1.06 Å. Excluding 127 intra-ligand and ligand-protein distance restraints, there are 591 more intra-protein distance restraints used in the final structure calculation of holo-CRBP II than apo-CRBP II (Lu *et al.*, 1999). Among them, 35 are intra-residue restraints, 126 are sequential restraints, 150 are medium-range restraints and 280 are long-range restraints. A sausage representation of the mean C^{α} coordinates of the holo and apo structure ensembles shown in Figure 6 illustrates the differences in detail. The apo-CRBP II structure is less well defined than the holo-CRBP II structure in the region of αII and the adjacent linker to the β-strand B, residues 57-62 in the βC-βD loop and residues 72-76 in the βE-βF loop. However, the NMR *B*-fac-

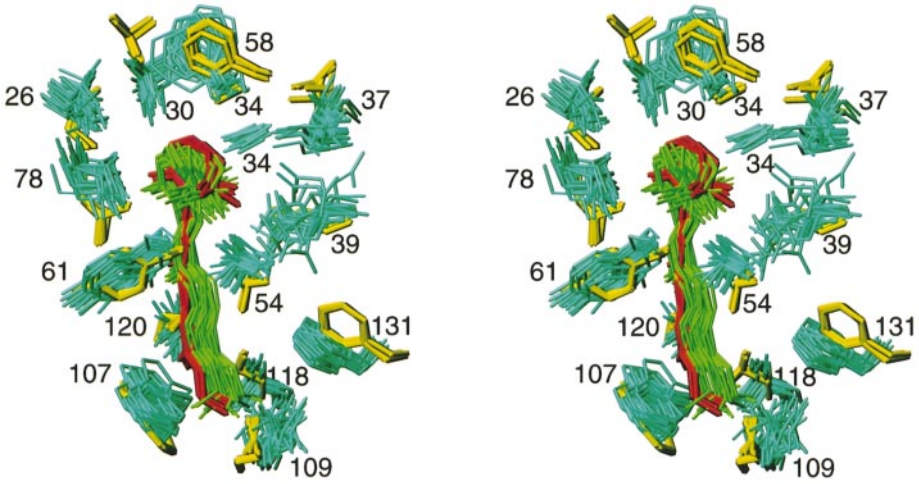

Figure 5. A stereodiagram of the bound retinols in the NMR ensemble (in green) superimposed on those in the crystal structures (in red). Residues that have NOE contacts with the ligand are shown in cyan along with the respective residues in the crystal structure (in yellow). Residues 20, 21, 24 (underneath the β-ionone ring of the bound retinol), 41, 59, 60 (above the β-ionone ring) and 63 (above the polyene chain) are omitted to allow a clear view of the ligand and the binding cavity.

tor for residues 80-82 of the βE-βF loop in the holo structure exceeds that of the apo structure.

The NMR structure of holo-CRBP II diverges from the NMR structure of apo-CRBP II in the proposed portal region (framed by αII and the adjacent linker to βB, the βC-βD turn, and the βE-βF turn). First of all, residues 28-35 form an α-helix in the holo structure as predicted by the chemical shift indices method. NOE constraints detected between the methylene and methyl protons on the β-ionone ring of retinol with T30 and A34 results in closer positioning of αII to the binding cavity. An increased number of NOE constraints detected between T38 of βB and E10, M11 and E12 of βA, and between Q39 and M11, is the basis for the large displacement of L37 and T38 towards βA. NOE cross-peaks were detected between the phenyl side-chain ring of F58 and H^{α} of T30, H^{γ} of K32, as well as methyl substituents on the β-ionone ring of the bound retinol. This is in addition to the NOE cross-peaks with residues 33-35 and 37 that were also previously observed in the apo structure. Thus, binding of ligand has shifted the average orientation of the side-chain of F58 to coincide with that of the X-ray structures of holo (see Figure 5) and apo-CRBP II. Compared with the orientation of the F58 side-chain in the solution structure of apo-CRBP II (Lu *et al*., 1999), this side-chain now further blocks the entry into the binding cavity.

The gap between βD and βE in the holo structure is smaller than the gap in the apo structure. As shown in Figure 6, the C^{α}-C^{α} distance between residues F65 and F71, which are located in the lower part of the gap, is reduced by 1 Å. The C^{α}-C^{α} distance between residues R59 and G77, which are located in the upper part of the gap is reduced by 3 Å. Twenty-five inter-strand NOEs were detected in the upper part of the gap in holo-CRBP II, compared to only ten in the apo structure. In addition, ligand protein NOE constraints were detected for residues 54, 58-61 and 63 of the βC-βD loop and for L78 of the βE-βF loop. There is also a large backbone displacement of the βG-βH turn in holo-CRBP II relative to apo-CRBP II, which can be attributed partly to the tight coupling between the βG and βF strands.

Ligand-induced changes in backbone dynamics

To determine if the decreased regional disorder observed in the NMR structures of holo-CRBP II was due to changes in molecular flexibility, amide ^{15}N NMR relaxation parameters, T_1, T_2 and NOE values were measured for each residue at a field strength of 500 MHz, pH 6.5 and 25 °C (provided as Supplementary Material). Holo-CRBP II exhibited no significant elevation of T_1 or depression of NOEs, which are indicative of internal motions on a sub-nanosecond timescale. This was observed also for apo-CRBP II (Lu *et al*, 1999). However, unlike apo-CRBP II, which showed significantly depressed T_2 values for the amide protons corresponding to residues 30, 32, 34-36, 56, 58, 60 and 61, the T_2 values observed for holo-CRBP II are flat. The exception is a significant depression in the T_2 value for D114 in the βH-βI loop. These data suggest that backbone flexibility is markedly decreased upon ligand binding.

The model-free parameters were obtained based on the three-parameter (S^2, τ_e and $R_{ex,\ app}$) representation of the spectral density function and a globally optimized overall rotation time of 7.9(±0.1) ns. As shown in Figure 7(a), the S^2 values for most of the residues in holo-CRBP II are

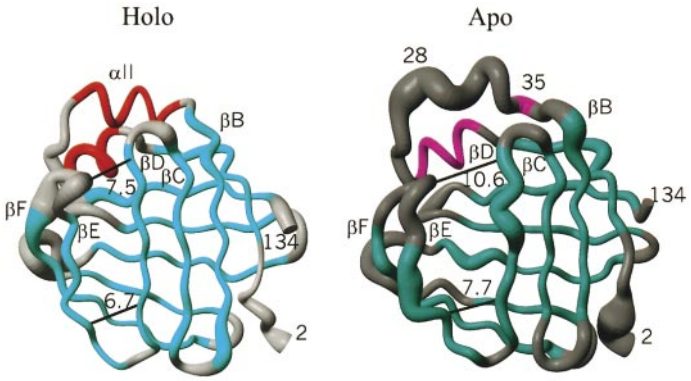

Figure 6. A ''sausage'' representation of the mean holo (left) and apo structures (right). The thickness of the sausage is defined by the NMR *B*-factor, which is the mean-square displacement multiplied by 8/3 * pi * pi (Koradi *et al.*, 1996). The α-helix, β-strand and coil are highlighted with red, cyan and gray, respectively. The two distances (in Å at the D-E gap) are between the α-carbon atoms of residues R59 and G77 as well as F65 and F71 (near the bottom).

between 0.8 and 0.9. This is very similar to the profile obtained for apo-CRBP II (Lu *et al.*, 1999) except for residues 3, 38, 60, 91, 102 and 113, which have S^2 values smaller than 0.7 in apo-CRBP II. These residues are located at the N terminus, the linker between αII and βB, the βC-βD, βF-βG, βG-βH and βH-βI turns. Thus, the elevated S^2 values of these residues upon ligand binding suggest that their backbone motions on the nanosecond time-scale are more restricted in holo than in apo-CRBP II. The $R_{ex,\ app}$ value was significantly increased for only residue D114 of holo-CRBP II (see Figure 7(b)). The $R_{ex,\ app}$ value for D114 was also increased for apo-CRBP II (Lu *et al.*, 1999). However no increase was observed in residues 28-40 corresponding to αII and adjacent linker to βB, and the βC-βD turn of the holoprotein.

Amide exchange on the millisecond to second timescale was measured by comparing relative peak intensities in gradient-enhanced 2D ^{1}H-^{15}N HSQC spectra collected with and without solvent presaturation at pH 7.4. The difference in the relative peak intensities with and without solvent presaturation observed for holo-CRBPII and apo-CRBP II is plotted in Figure 7(c). Two segments comprising residues 27, 30 and 32-35 in αII, and residues 57-59 in the βC-βD turn show a marked increase (0.3) of relative signal intensities upon ligand binding. Unfortunately, the residues in the βE-βF turn cannot be compared because of signal overlap. Thus, both amide exchange and relaxation data indicate that binding of retinol decreases backbone flexibility in the microsecond to second timescale in the region of αII and adjacent linker to βB, and in the region of the βC-βD turn.

Ligand-induced changes in protein conformation

Apo-CRBP II has a more expanded structure than holo-CRBP II because it has fewer NOE constraints, which are due, in part, to increased backbone flexibility on the microsecond to second timescale. Another important piece of independent evidence that binding of ligand induces changes in protein conformation comes from inspection of chemical shift perturbations. Two-site chemical exchange cross-peaks between the major and minor amide proton resonances corresponding to residues F28, I33 and R36 were observed in the 3D ^{15}N-resolved NOESY spectrum of apo-CRBP II. However, only a single resonance was observed for these amide protons in the corresponding spectrum of holo-CRBP II. The ^{1}H and ^{15}N chemical shifts of residues F28, I33 and R36 in holo-CRBP II more closely approximate the chemical shifts of the minor resonances than the major resonances of these three residues in apo-CRBP II (see Table 2). The detection of a limited number of HN_{i+2}-HN_i and HN_{i+3}-H^{α}_i NOEs identified between the minor resonances, but not between the major resonances, suggested that the less populated conformation for the apoprotein is helical and the more populated conformation is a random coil. A comparison of the chemical shift consensus indices corresponding to residues 28-34 in holo-CRBP II (see Figure 4), with those for apo-CRBP II (Lu *et al.*, 1999) indicate that this region of the protein undergoes a coil to helix transition on binding retinol. Although the more extended conformation of the βC-βD and βE-βF turn in apo-CRBP II may reflect

Table 2. Comparison of the amide ^{1}H and ^{15}N chemical shifts of residues 28, 33 and 36 in the major and minor forms of apo-CRBP II with those of holo-CRBP II measured at pH 6.5 and 25 °C

Residue	Major form Δδ (ppm)	Minor form Δδ (ppm)
F28	0.09	0.03
I33	0.26	0.05
R36	0.47	0.09
All[a]	0.12	-

$\Delta\delta = \sqrt{(((\delta^{apo}_{HN} - \delta^{holo}_{HN})^2 + (\delta^{apo}_{N} - \delta^{holo}_{N})^2/25)/2)}$, where $\delta^{apo/holo}_{HN}$ and $\delta^{apo/holo}_{HN}$ are the HN and N chemical shifts of apo and holo-CRBP II.

[a] It includes all the residues shown in Figure 4(a) and the value is the mean of all.

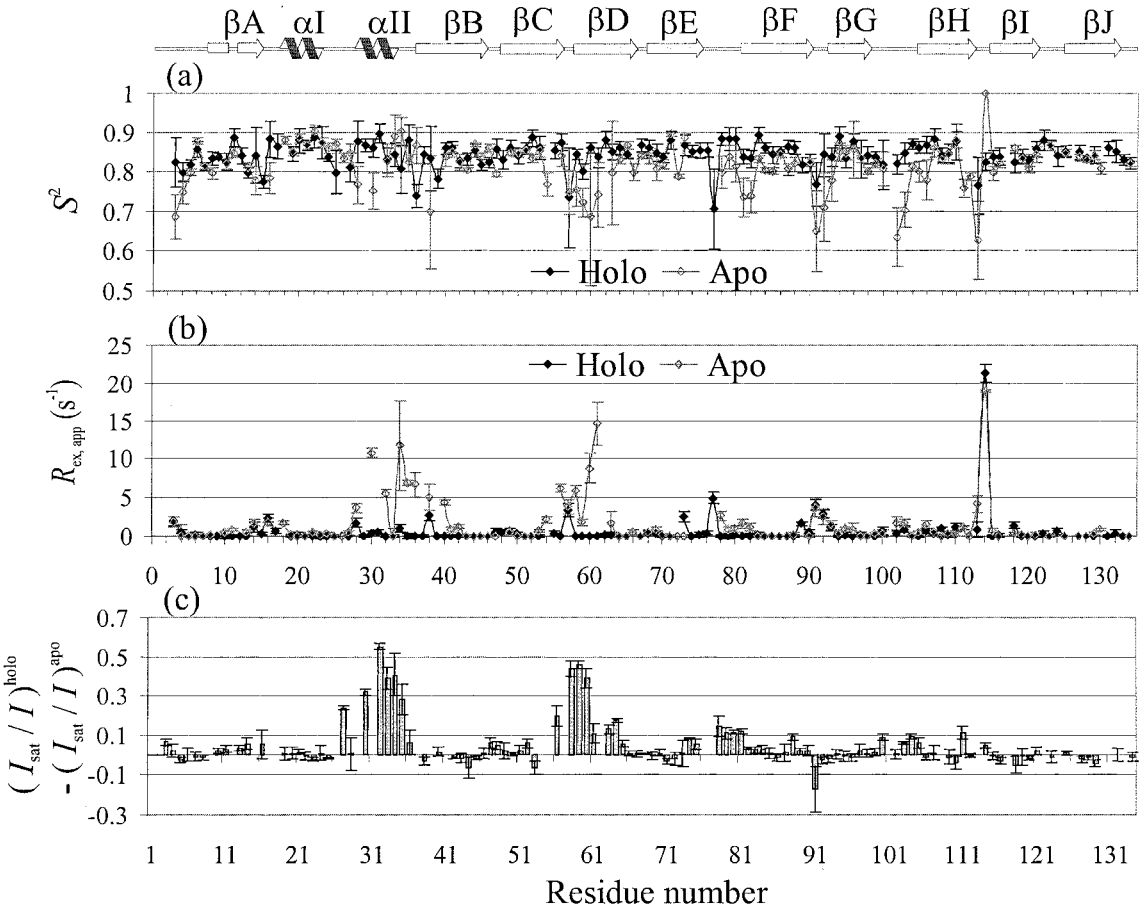

Figure 7. (a) Histogram of the generalized order parameter S^2 of holo and apo-CRBP II derived from the ^{15}N-relaxation parameters using the three-parameter (S^2, τ_e and $R_{ex, app}$) models. The ^{15}N-relaxation parameters were measured at a 500 MHz magnet, pH 6.5 and 25 °C. Omitted values were due to severe signal overlaps rather than missing assignments, except for those of residues 1 and 2 in both forms and 39 in the apo form. (b) Histogram of the conformational exchange rate $R_{ex, app}$ overlaid with those of the apo-CRBP II. Note that the R_{ex} described here is not the true R_{ex}, but an apparent one, which contains contributions from amide exchange in addition to the true R_{ex}. (c) Difference of the saturation transfer rate between holo and apo-CRBP II 25 °C and pH 7.4. The saturation transfer rate is defined as the relative intensity of a backbone amide proton signal with and without solvent saturation.

the decreased number of NOE restraints observed in this region, an inspection of the chemical shift map (see Figure 3) suggests that these regions undergo changes in conformation upon binding retinol.

Structural basis for differences in the ligand protein interactions of CRBP II and CRBP

CRBP and CRBP II exhibit differences in their pattern of tissue expression during development, suggesting that they serve different physiological functions (Ong *et al.*, 1994; Li & Norris, 1996). CRBP is located in many tissues but is most abundant in liver, kidney and testis. CRBP is essential for storage of retinol in the liver, particularly when animals are fed a vitamin A-deficient diet (Ghyselinck *et al.*, 1999). CRBP II is localized within the absorptive intestinal epithelial cells and in perinatal hepatocytes (Ong *et al.*, 1994; Li & Norris, 1996). This suggests that it may play a role in vitamin A absorption, and may also play an important role in the maternal-fetal transfer of all-*trans*-retinol. CRBP and CRBP II differ in their ligand binding affinities for all-*trans*-retinol, ligand binding specificity, and the mechanism of retinol transfer to phospholipid membranes. CRBP II binds retinol with an affinity that is at least an order of magnitude less than the retinol-binding affinity of CRBP (Li *et al.*, 1991; Herr *et al.*, 1999). Retinol analogs lacking the ring methyl substituents fail to bind CRBP II but bind tightly to CRBP (Rong *et al.*, 1993). Transfer of retinol from CRBP II to phospholipid vesicles is independent of vesicle concentration or phospholipid composition, whereas transfer of retinol from CRBP to phospholipid vesicles increases with increasing vesicle

concentration and with the incorporation of anionic lipids such as cardiolipin or phosphatidylserine in the vesicles (Herr *et al*., 1999). These results suggest that transfer of retinol from CRBP II involves diffusion through the aqueous solution. In contrast, transfer of retinol from CRBP to phospholipid vesicles requires direct contact between the protein and membrane in order to release the bound retinol.

We hypothesize that release of retinol from the binding pocket is triggered by perturbation of the helix-turn-helix motif. The structural basis for differences in ligand-binding properties of CRBP and CRBP II ultimately resides in the sequence divergence between the two proteins. There are 58 of 133 positions where the sequence of rat CRBP II differs from that of rat CRBP, and these positions are distributed throughout the length of the protein. However a number of positions are clustered in the helix-turn-helix motif and the adjacent linker to βB. These mutations from CRBP II to CRBP include M21(L), K22(R), I26(V), D27(N), F28(V), T30(L), V35(N), R36(L), T38(K), and Q39(P). M21, I26, T30 and Q39 of CRBP II are predicted to be in close proximity to the ring methyl substituents of bound retinol. Removal of these substituents abolishes retinol binding to CRBP II but not to CRBP. What remains to be determined is whether the sequence divergence in this region accounts for the differences in CRBP and CRBP II ligand-binding properties. It is likely that no single substitution is sufficient, since single mutations of CRBP in this region resulted in relatively modest alterations in ligand-binding affinity (Penzes & Napoli, 1999). However, substitution of the helix-turn-helix motif of CRBP II with that of CRBP may significantly increase its binding affinity for retinol and alter its interactions with lipid membranes.

It remains to be determined whether the second helix of CRBP locally unfolds in the apo form in solution. Molecular dynamics and essential dynamics (ED) simulations of CRBP indicate that, on binding all-*trans*-retinol, the βC-βD loop, the βE-βF loop and αII from the helix-turn-helix motif move towards each other and close the entrance to the ligand-binding site (van Aalten *et al*., 1995). This motion is part of the ''essential space'' of both holo-CRBP and apo-CRBP, but is predicted to be far more restricted in holo-CRBP than in apo-CRBP. The essential motions in holo-CRBP and apo-CRBP show a concerted motion of these elements, which are facilitated by the presence of two hinges, located at residues corresponding to G68 and T38 of CRBP II. The crystal structure of holo but not apo-CRBP has been reported; however, the coil to helix transition was not observed in the crystal structures of apo and holo-CRBP II. Studies are underway to determine the solution structure of apo-CRBP and to determine whether exchanging the residues comprising the second helix significantly alter the ligand-binding properties of these two proteins.

Materials and Methods

Sample preparation

The expression, purification and delipidation of ^{13}C,^{15}N-enriched, ^{15}N-enriched and natural abundance CRBP II proteins have been described (Lu *et al*., 1999). A holo-CRBP II sample used in the NMR study was prepared as described (Norris *et al*., 1995). The phosphate buffer with pH 7.4 or pH 6.5 was prepared in the same way as that for apo-CRBP II (Lu *et al*., 1999). The final concentrations of the NMR samples were usually between 1.0 and 2.0 mM, unless specified otherwise (see the next section).

Preparation of (2,3,6,7,8,9,10,11,19-^{13}C)-all-*trans*-retinol

A sub-milligram amount of (2,3,6,7,8,9,10,11,19-^{13}C)-all-*trans*-retinoic acid bound to natural abundance CRABP I and CRABP II (Norris *et al*., 1995) was extracted with hexane and a 2:1 mix of hexane and ethyl acetate as described (Napoli & Horst, 1998). The N_2 gas-dried extract was mixed with 100-fold molar excess of diisobutylaluminum hydride in hexane (Aldrich, Milwaukee, WI) at 0 °C, as described (Rong *et al*., 1993). After five hours, the reaction was quenched with ice-water, and the product (2,3,6,7,8,9,10,11,19-^{13}C)-all-*trans*-retinol (ligand **2**) was extracted with ethyl acetate. The conversion rate was over 96 %, as measured by HPLC, and no further purification was necessary. A total of 22 μg of ligand **2** was obtained and used to make a ~0.2 mM holo-CRBP II NMR sample for resonance assignments of the bound ligand.

NMR spectroscopy

The NMR experiments were carried out at 25 °C on either a Varian UNITY or UNITYplus 500 MHz spectrometer equipped with an actively shielded Z-gradient probe and a gradient amplifier unit. The sequence-specific resonance assignments and the 3D structure determination were carried out on ^{13}C,^{15}N-enriched holo-CRBP II samples at pH 7.4. For backbone resonance assignments, six triple-resonance 3D spectra were recorded, including HNCO (Muhandiram & Kay, 1994), HNCACB (Muhandiram & Kay, 1994), TOCSY-HMQC, CBCACO(CA)HA (Kay, 1993a), HCA(CO)N (Powers *et al*., 1991) and CBCA(CO)NNH (Muhandiram & Kay, 1994). For side-chain resonance assignments, 3D HCCH-TOCSY (Bax *et al*., 1990) and CC-TOCSY (Kay, 1993b) spectra were recorded. For structure determination, 3D ^{13}C-resolved and ^{15}N-resolved (Zhang *et al*., 1994) NOESY-HSQC spectra were recorded. For the ^{1}H and ^{13}C resonance assignment of the bound all-*trans* retinol, ^{13}C double-tuned Z-gradient filtered DQF-COSY and TOCSY (Ogura *et al*., 1996) spectra were recorded on natural abundance all-*trans*-retinol bound to ^{13}C,^{15}N-enriched CRBP II at pH 7.4, and a ^{1}H,^{13}C HMQC spectrum was recorded on ligand **2** bound to natural abundance CRBP II at pH 7.4. For the identification of protein-ligand interaction, a ^{13}C,^{15}N double-half-filtered NOE experiment (Slijper *et al*., 1996) was carried out on natural abundance all-*trans*-retinol bound to ^{13}C,^{15}N-

enriched CRBP II at pH 7.4. The assignment of the backbone HN and side-chain proton resonances at pH 6.5 was made in the 3D ^{15}N-resolved TOCSY-HSQC and NOESY-HSQC spectra recorded on an ^{15}N-enriched protein sample at pH 6.5. This sample was subsequently used for ^{15}N relaxation measurements in a way similar to that described previously (Hodsdon & Cistola, 1997b). The relaxation delays for T_1 measurement were 22.3(3), 55.8, 112, 168(3), 223, 279, 335, 447, 558, 670 and 782 ms, and those for T_2 measurement were 15.5(2), 31.0, 46.6, 62.1, 77.6, 93.1, 109, 140 and 171(2) ms. The steady-state {^{1}H}^{15}N NOE spectrum and its reference spectrum were measured in three pairs. The saturation transfer spectrum and its reference spectrum were recorded in three pairs at both pH 7.4 and 6.5. The ^{1}H, ^{13}C and ^{15}N chemical shifts were referenced as described (Lu *et al*., 1999).

Restraint derivation and structure calculations

The procedure for the derivation of intra-protein distance and dihedral angle restraints has been described (Lu *et al*., 1999). The NOE constraint lists were constructed from the cross-peaks in 3D ^{13}C-resolved and ^{15}N-resolved NOESY-HSQC spectra and 2D ^{13}C,^{15}N double-half-filtered NOE spectra using a tolerance of 0.04 ppm. The dihedral angles of the five double bonds in all-*trans*-retinol were fixed at 180(±5)°. The dihedral angles of the four single bonds (6-s, 8-s, 10-s and 12-s) were fixed at 180(±60)° (see Results and Discussion). For protein-ligand interaction, six unique NOE constraints between L78 H$^\delta$ of the protein and H8, H12, H16, H17, H18, H19 of the ligand were initially identified. Other inter-ligand-protein NOEs were gradually interpreted based on the NMR working model. The structure calculations were performed on a Silicon Graphics O2/R10000 workstation, using DISTGEOM, a unique distance geometry/simulated annealing algorithm implemented in the TINKER protein modeling package described by Hodsdon *et al*. (1996). The calculation was usually carried out to yield 25 structures for statistical analysis of the distance restraint violation. Restraints whose upper bounds were violated in more than five of the 25 structures were removed. A total of 2338 distance restraints obtained manually in a systematic fashion (Lu *et al*., 1999) were used to establish the initial global fold. These include 864 intra-residue, 895 sequential, 123 medium-range, 456 long-range and 18 protein-ligand distance restraints. After a six-round iterative filtering procedure (Hodsdon *et al*., 1996), 3223 distance restraints were obtained automatically. Subsequently, the remaining unassigned cross-peaks were sorted out and inspected in the spectra. They were interpreted based on the NMR working model, given the same tolerance of 0.04 ppm. In the rest of the iterative calculations, these unassigned cross-peaks would be interpreted as much as possible. In addition, effort was made to maintain the regular secondary structures, in particular the β-strands, and improve the stereochemical quality of the protein structures. A total of 16 rounds of iterative calculations were carried out to obtain the final structures. In the final calculation, 30 structures were generated and 25 of them were within two standard deviations from the average penalty function value. These 25 structures were accepted as the final structures and the corresponding average penalty function value was 0.10 ± 0.10.

Relaxation and model-free parameter calculations

The ^{15}N relaxation parameters T_1, T_2, steady-state NOE were calculated as described (Farrow *et al*., 1994; Hodsdon & Cistola, 1997b). Backbone dynamics was derived from the ^{15}N relaxation parameters using Farrow's software (1994) written based on the model-free formalism. The generalized order parameter S^2, effective correlation time τ_e and the apparent exchange rate $R_{ex,\ app}$ were used to fit the relaxation parameters of all residues in holo-CRBP II in the same way as in the study of apo-CRBP II.

Protein Data Bank and BioMagResBank accession numbers

The coordinates of the final 25 structures of apo-CRBP II and the distance restraints used to calculate the final ensemble have been deposited in the RCSB Protein Data Bank with accession number 1EII. The chemical shifts for both apo and holo-CRBP II have been deposited in the BioMagResBank with accession number 4681 and 4682, respectively.

Acknowledgments

This work was supported by Washington University Digestive Diseases Research Core Center (DK 52574)-Protein Structure and Macromolecular Graphics Core, grants from the National Institutes of Health, DK 40172 and DK 49684 (to E. L.) and a grant from the National Science Foundation, DBI9808317. E. L. is a Burroughs Wellcome Scholar in Toxicology. The Molecular Biophysics NMR Laboratory and the Unity-500 spectrometer was supported, in part, by the Markey Center for Research in the Molecular Biology of Disease at Washington University. Spectra were also collected at the Washington University High Resolution NMR Service Facility, which is funded, in part, through National Institutes of Health Biomedical Research Support Shared Instrument grants RR-02004, -05018 and -07155. We thank Dr Michael E. Hodsdon for providing the C codes and scripts for the structural analysis, Dr James J. Toner for his help in protein isotope labeling, Mr Alex Maldonado for the ^{15}N-labeled protein purification, Dr Lewis E. Kay for providing the pulse sequences of the triple resonance experiments, Dr Neil A. Farrow for providing the relaxation analysis software, and Drs Gregory DeKoster and Ruth Steele for critical reading of the manuscript. Information and software for the TINKER package can be obtained at www.dasher.wustl.edu.

References

Bax, A., Clore, G. M. & Gronenborn, A. M. (1990). ^{1}H-^{1}H correlation via isotropic mixing of ^{13}C magnetization, a new three-dimensional approach for assigning ^{1}H and ^{13}C spectra of ^{13}C-enriched proteins. *J. Magn. Reson.* **88**, 425-431.

E, X., Zhang, L., Davis, A. E., Levin, M. S. & Li, E. (1999). Generation of cellular retinol binding protein II in knockout mice. In *The 100th Annual Meeting of the American Gastroenterological Association, Orlando, FL*, W. B. Saunders Company, Philadelphia, PA.

Farrow, N. A., Muhandiram, R., Singer, A. U., Pascal, S. M., Kay, C. M., Gish, G., Shoelson, S. E., Pawson, T., Forman-Kay, J. D. & Kay, L. E. (1994). Backbone dynamics of a free and phosphopeptide-complexed Src homology 2 domain studied by ^{15}N NMR relaxation. *Biochemistry,* **17**, 5984-6003.

Ghyselinck, N. B., Bavik, C., Sapin, V., Mark, M., Bonnier, D., Hindelang, C., Dierich, A., Nilsson, C. B., Hakansson, H., Sauvant, P., Azais-Braesco, V., Frasson, M., Picaud, S. & Chambon, P. (1999). Cellular retinol-binding protein I is essential for vitamin A homeostasis. *EMBO J.* **18**, 4903-4914.

Güntert, P., Mumenthaler, C. & Wüthrich, K. (1997). Torsion-angle dynamics for NMR structure calculation with the new program DYANA. *J. Mol. Biol.* **273**, 283-298.

Harbison, G. S., Smith, S. O., Pardoen, J. A., Courtin, J. M. L., Lugtenburg, J., Herzfeld, J., Mathies, R. A. & Griffin, R. G. (1985). Solid-state ^{13}C NMR detection of a perturbed 6-s-trans chromophore in bacteriorhodopsin. *Biochemistry,* **24**, 6955-6962.

Herr, F. M. & Ong, D. E. (1992). Differential interaction of lecithin-retinol acyltransferase with cellular retinol binding proteins. *Biochemistry,* **31**, 6748-6755.

Herr, F. M., Li, E., Weinberg, R. B., Cook, V. R. & Storch, J. (1999). Differential mechanisms of retinoid transfer from cellular retinol binding proteins types I and II to phospholipid membranes. *J. Biol. Chem.* **274**, 9556-9563.

Hodsdon, M. E. & Cistola, D. P. (1997a). Discrete backbone disorder in the NMR structure of apo intestinal fatty acid-binding protein in solution: implications for the mechanism of ligand entry. *Biochemistry,* **36**, 1450-1460.

Hodsdon, M. E. & Cistola, D. P. (1997b). Ligand binding alters the backbone mobility of intestinal fatty acid-binding protein as monitored by ^{15}N NMR relaxation and ^{1}H exchange. *Biochemistry,* **36**, 2278-2290.

Hodsdon, M. E., Ponder, J. W. & Cistola, D. P. (1996). The NMR solution structure of intestinal fatty acid-binding protein complexed with palmitate: application of a novel distance geometry algorithm. *J. Mol. Biol.* **264**, 585-602.

Honig, B., Hudson, B., Sykes, B. D. & Karplus, M. (1971). Ring orientation in β-Ionone and retinals. *Proc. Natl Acad. Sci. USA,* **68**, 1289-1293.

Jamison, R. S., Newcomer, M. E. & Ong, D. E. (1994). Cellular retinoid-binding proteins: limited proteolysis reveals a conformational change upon ligand binding. *Biochemistry,* **33**, 2873-2879.

Kay, L. E. (1993a). Pulsed-field gradient-enhanced three-dimensional NMR experiment for correlating ^{13}Ca/b, ^{13}C′, and ^{1}Ha chemical shifts in uniformly ^{13}C-labeled proteins dissolved in H_2O. *J. Am. Chem. Soc.* **115**, 2055-2057.

Kay, L. E. (1993b). A three-dimensional NMR experiment for the separation of aliphatic carbon chemical shifts via the carbonyl chemical shift in ^{15}N, ^{13}C-labeled proteins. *J. Magn. Reson. Ser. B,* **101**, 110-113.

Koradi, R., Billeter, M. & Wüthrich, K. (1996). MOLMOL: a program for display and analysis of macromolecular structures. *J. Mol. Graph.* **14**, 51-55.

Laskowski, R. A., MacArthur, M. W., Moss, D. S. & Thornton, J. M. (1993). PROCHECK: A program to check the stereochemical quality of protein structures. *J. Appl. Crystallog.* **26**, 283-291.

Laskowski, R. A., Rullmann, J. A. C., MacArthur, M. W., Kaptein, R. & Thornton, J. M. (1996). AQUA and PROCHECK-NMR: programs for checking the quality of protein structures solved by NMR. *J. Biomol. NMR,* **8**, 477-486.

Li, E. & Norris, A. W. (1996). Structure/function of cytoplasmic vitamin A-binding proteins. *Annu. Rev. Nutr.* **16**, 205-234.

Li, E., Qian, S. J., Winter, N. S., d'Avignon, A., Levin, M. S. & Gordon, J. I. (1991). Fluorine nuclear magnetic resonance analysis of the ligand binding properties of two homologous rat cellular retinol-binding proteins expressed in *Escherichia coli*. *J. Biol. Chem.* **266**, 3622-3629.

Liu, R. S. H. & Asato, A. E. (1984). Photochemistry and synthesis of stereoisomers of vitamin A. *Tetrahedron,* **40**, 1931-1969.

Lu, J., Lin, C. L., Tang, C., Ponder, J. W., Kao, J. L. F., Cistola, D. P. & Li, E. (1999). The structure and dynamics of rat apo-cellular retinol-binding protein II in solution: comparison with the X-ray structure. *J. Mol. Biol.* **286**, 1179-1195.

Muhandiram, D. R. & Kay, L. E. (1994). Gradient-enhanced triple-resonance three-dimensional NMR experiments with improved sensitivity. *J. Mag. Reson. ser. B,* **103**, 203-216.

Napoli, J. L. & Horst (1998). Quantitative analyses of naturally occurring retinoids. In *Methods in Molecular Biology: Retinoid Protocols* (Redfern, C. P. F., ed.), vol. 89, pp. 29-40, Humana Press Inc., Totowa, NJ.

Norris, A. W., Rong, D., d'Avignon, D. A., Rosenberger, M., Tasaki, K. & Li, E. (1995). Nuclear magnetic resonance studies demonstrate differences in the interaction of retinoic acid with two highly homologous cellular retinoic acid binding proteins. *Biochemistry,* **34**, 15564-15573.

Ogura, K., Terasawa, H. & Inagaki, F. (1996). An improved double-tuned and isotope-filtered pulse scheme based on a pulsed field gradient and a wide-band inversion shaped pulse. *J. Biomol. NMR,* **8**, 492-498.

Ong, D. E., Newcomer, M. E. & Chytil, F. (1994). Cellular retinoid binding proteins. In *The Retinoids: Biology, Chemistry, and Medicine* (Sporn, M. B., Robert, A. B. & Goodman, D. S., eds), 2nd edit., pp. 283-312, Raven Press Ltd., New York.

Pellecchia, M., Sebbel, P., Hermanns, U., Wuthrich, K. & Glockshuber, R. (1999). Pilus chaperone FimC-adhesin FimH interactions mapped by TROSY-NMR. *Nature Struct. Biol.* **6**, 336-339.

Penzes, P. & Napoli, J. L. (1999). Holo-cellular retinol-binding protein: distinction of ligand-binding affinity from efficiency as substrate in retinal biosynthesis. *Biochemistry,* **38**, 2088-2093.

Powers, R., Gronenborn, A. M., Clore, G. M. & Bax, A. (1991). Three-dimensional triple-resonance NMR of ^{13}C/^{15}N-enriched proteins using constant-time evolution. *J. Magn. Reson.* **94**, 209-213.

Rong, D., Lovey, A. J., Rosenberger, M., d'Avignon, D. A., Ponder, J. W. & Li, E. (1993). Differential binding of retinol analogs to two homologous cellular retinol-binding proteins. *J. Biol. Chem.* **268**, 7929-7934.

Slijper, M., Kaptein, R. & Boelens, R. (1996). Simultaneous ^{13}C and ^{15}N isotope editing of biomolecular complexes. Application to a mutant *Lac* repressor headpiece DNA complex. *J. Magn. Reson. ser. B,* **111**, 199-203.

Stein, E. G., Rice, L. M. & Brünger, A. T. (1997). Torsion-angle molecular dynamics as a new efficient tool for NMR structure calculation. *J. Magn. Reson.* **124**, 154-164.

van Aalten, D. M. F., Findlay, J. B. C., Amadei, A. & Berendsen, H. J. C. (1995). Essential dynamics of the cellular retinol-binding protein - evidence for ligand-induced conformational changes. *Protein Eng.* **8**, 1129-1135.

Winter, N. S., Bratt, J. M. & Banaszak, L. J. (1993). Crystal structures of holo and apo-cellular retinol-binding protein II. *J. Mol. Biol.* **230**, 1247-1259.

Wishart, D. S. & Sykes, B. D. (1994). The ^{13}C chemical-shift index: a simple method for the identification of protein secondary structure using ^{13}C chemical-shift data. *J. Biomol. NMR,* **4**, 171-180.

Zhang, O., Kay, L. E., Olivier, J. P. & Forman-Kay, J. D. (1994). Backbone ^{1}H and ^{15}N resonance assignments of the N-terminal SH3 domain of drk in folded and unfolded states using enhanced-sensitivity pulsed field gradient NMR techniques. *J. Biomol. NMR,* **4**, 845-858.

Edited by P. E. Wright

(Received 25 February 2000; received in revised form 3 May 2000; accepted 17 May 2000)

http://www.academicpress.com/jmb

Supplementary material comprising one Figure and two pages is available from JMB Online